08

Three-stage synthesis of composite nanomaterials based on iron and gold by laser ablation and assisted ultrasound

© A.S. Chernikov, D.A. Kochuev, R.V. Chkalov, M.A. Dzus, E.I. Shingareva, K.S. Khorkov

Vladimir State University,
600000 Vladimir, Russia
e-mail: khorkov@vlsu.ru

Received December 9, 2025
Revised December 9, 2025
Accepted December 9, 2025

The paper presents the results of a three-stage synthesis of composite nanoparticles based on a combination of femtosecond laser ablation and ultrasound exposure. The synthesis was carried out by laser ablation in deionized water and by laser ablation in a gaseous medium (argon or air) in the presence of a magnetic or electrostatic field. The approach used leads to the formation of composite magneto-plasmon nanoparticles with a „core–satellite“configuration. For the two types of composite nanoparticles under consideration, a redshift of the plasmon resonance position is observed from 520 nm (initial gold nanoparticles) to 545−548 nm (composite magneto-plasmon nanoparticles). The heating of solutions of composite Fe_3O_4–Au and PVP α-Fe–Au with concentrations of 0.06 mg/ml and 0.07 mg/ml was 10.6 °C and 10.6 °C, respectively. The experimental data obtained confirm the possibility of using the proposed combined approach to create composite nanoparticles with magnetic and plasmonic properties. This approach allows flexible variation of synthesis conditions to obtain nanoparticles with the necessary properties.

Keywords: Keywords: laser ablation, laser fragmentation, magnetic nanoparticles, gold nanoparticles, composite nanoparticles, photothermal response, magneto-plasmon nanoparticles.

DOI: 10.61011/TP.2026.05.63524.333-25

Introduction

The combination of synthesis and formation control methods for the nanoparticles (NP) of specified parameters opens up the prospects for fabrication of the new types of materials. Laser ablation in liquids makes it possible to synthesize composite nanoparticles by ablating multilayer targets or bulk alloys, obtaining metastable alloys, „core-satellites“ structures or bimetallic particles with controlled size and composition [1–4]. Getting the nanoparticls featuring these combined properties is an expected progress in development of the monitored and controlled synthesis technologies. NP with pronounced magnetic and photo-sensitized properties are used for hyperthermia, which is a relevant issue in modern biology and medicine [5–8]. Plasmonic photothermal properties of gold nanoparticles are widely studied in biomedicine to provide a photothermal effect in response to irradiation with an external light source [9]. In today's oncological research, there is a steady transition from monotherapy to combined kinds of therapy that demonstrate significantly higher efficacy. Hybrid multimodal NP are used as contrast agents for dual magnetic resonance imaging and computer tomography, as well as sensitizers for laser-induced hyperthermia of cancer cells [10]. The promising trend is the integration of magnetic hyperthermia with other therapeutic modalities, including photothermal, photodynamic, radiation therapy, immunotherapy and chemotherapy. This offers a challenge to develop multifunctional platforms based on magnetic NP designed to enhance the synergistic effect of a combined therapy to achieve maximum antitumor efficacy with a minimum level of adverse reactions [11–13]. The size of NP impacts the relaxation properties of protons in biological fluids and tissues, so it is necessary to trace the dependence of the nanopraticles' dimensional and structural parameters when treating the biological objects. The combination of magnetic and photosensitized properties in composite NP obtained by laser synthesis opens up opportunities for creating universal platforms for simultaneous diagnosis, targeted delivery and combined therapy [14–18].

This study is aimed at getting composite magneto-plasmon nanoparticles based on iron and gold with a „core–satellite“„configuration using a three-step synthesis. Magnetic nanopraticles Fe_3O_4 or α-Fe serve as a core, and golden NP — as satellites. The proposed approach is based on a combination of femtosecond laser ablation to obtain the initial NP and ultrasound exposure to form composite NP. The method of magnetic separation in a liquid medium was used for purification and selection of target products.

1. Materials and experimental diagrams

The three-stage synthesis used is based on a combination of laser ablation and ultrasound methods. The femtosecond laser system Yb:KGW (Avesta, Russia) was used as a radiation source in experiments on laser ablation synthesis: radiation wavelength 1030 nm, maximum pulse energy

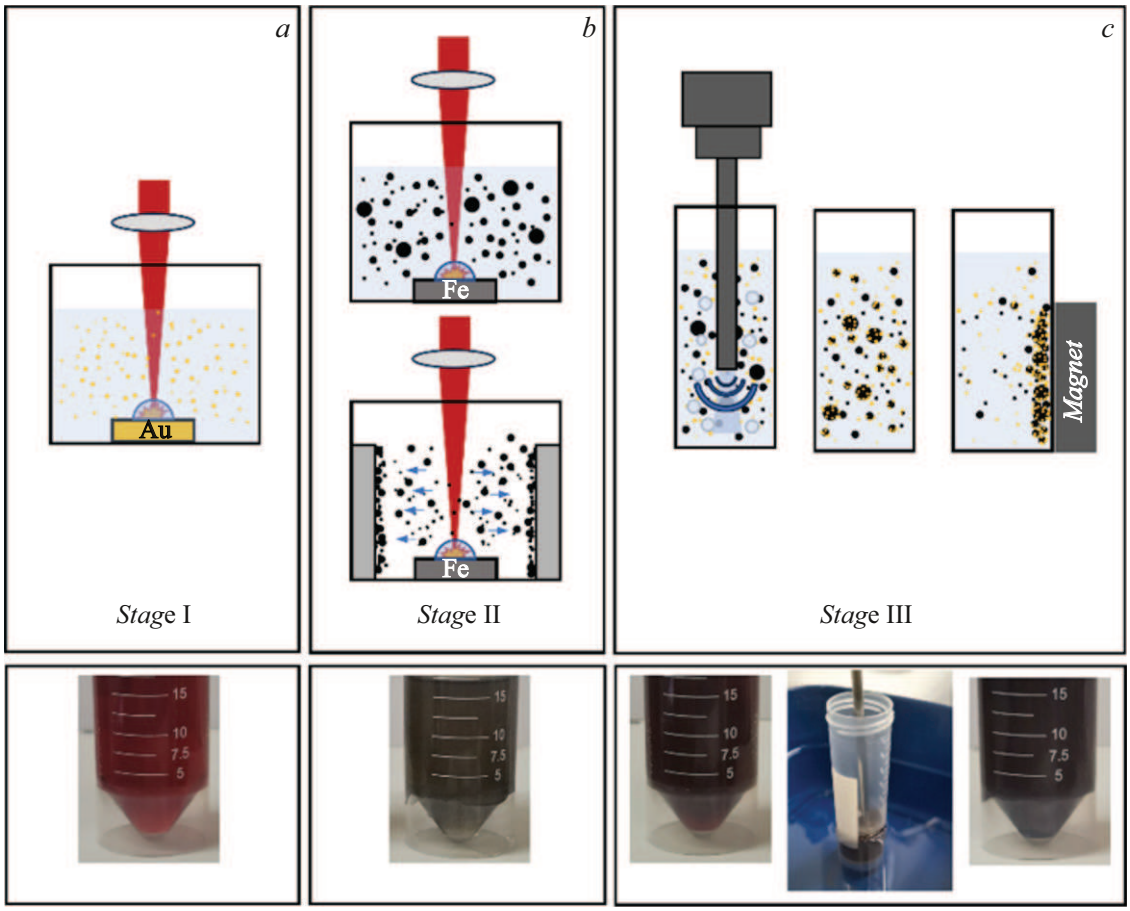

Figure 1. Schematic representation of a three-stage synthesis of composite iron-gold nanomaterials using laser ablation and assisted ultrasound exposure. *a* — synthesis of gold NP; *b* — synthesis of magnetic NP; *c* — Ultrasonic effect on a mixture of solutions.

150 μJ, pulse duration 280 fs, pulse repetition rate 10 kHz. Scanning with a laser beam over the target surface during laser ablation and fragmentation in a liquid medium was carried out using a hboxX–Y galvanoscanner, focusing was carried out using hboxF-theta lens with an operating distance of 200 mm. Deionized water was used as a liquid medium. High purity iron and gold ($> 99.95\,\%$) were used as targets in the experiments.

A schematic representation of the three-stage synthesis process of composite nanomaterials based on iron and gold by laser ablation and assisted ultrasound is shown in Fig. 1.

The first stage included synthesis of colloidal solutions of golden NP (Fig. 1, *a*). The target was placed in a cuvette filled with 1 mmol of NaCl solution. Scanning with a laser beam over the target surface was performed using a galvanoscanner, the energy in the pulse was set at 30 μJ, process duration ranged from 30 to 90 min, depending on the volume. Concentration of the obtained colloidal solution was around 0.125 mg/ml. To select particles of minimum size, a centrifugation was used. After the process was completed, the supernatant liquid was collected and used in further experiments. As an alternative to the centrifugation stage, the method of femtosecond laser fragmentation in a liquid medium could be used (pulse energy 100 μJ, process duration 30 min). As a result of laser fragmentation, the total number of gold nanoparticles rises due to the transformation of large particles into many smaller ones. This leads to the size distribution shift towards smaller diameters, which manifests itself in a blue shift in the position of the plasmon resonance and a decrease in optical density in the long-wavelength region of the spectrum, while maintaining the initial mass concentration of the colloidal solution. Maintaining the mass concentration is a significant advantage compared to centrifugation of the initial solution. In case of centrifugation, a significant portion of the material is removed as sediment, and the target fraction remains in the supernatant liquid, which ultimately leads to a decrease in the mass concentration of the colloidal solution.

The objective was to obtain the NP with magnetic properties (Fig. 1, *b*). The synthesis was carried out by laser ablation in deonized water and by laser ablation in a gaseous medium (argon or air) in the presence of a magnetic or electrostatic field [19,20]. In both cases, the next step was the selection of NP with magnetic properties, which was carried out by magnetic separation in a liquid medium (acetone for NP synthesized in argon and deionized water for all other NP).

Experiments on laser ablation of an iron target in a gaseous environment (argon, air) were carried out in an isolated vessel. When using argon, the vessel was pumped with a flow rate of 1 l/min, the ablation process began 5 min after the start of pumping. During the laser ablation synthesis process, the gas flow rate did not change. Ablation products were removed from the affected area and their predicted deposition was carried out under the influence of electrostatic or magnetic fields, depending on the vessel configuration used (electrodes or permanent magnets). The configuration was changed through minimal design changes. The target was placed between parallel electrodes or permanent magnets. The energy of pulse was about 50 μJ.

The electrostatic field between the electrodes was created by a high voltage source and varied in the range from 6 to 60 kV through high-voltage electrical inputs located on the wall of an insulated vessel. Permanent magnets (maximum magnetic field 3000 G) with fixed quartz substrates were positioned with similarly charged poles facing each other. When the synthesis is completed, the ablation products deposited on the surface of the electrodes or quartz plates (under the action of electrostatic and magnetic fields, respectively) were collected using a spatula and placed in pre-weighed tubes. When conducting experiments in air, effective removal of ablation products and their predicted deposition is possible in the presence of electrostatic or magnetic fields. When using argon, effective deposition of ablation products is possible only in the presence of a magnetic field; in the presence of an electrostatic field, ablation products were observed to hover between the electrodes and move through the vessel without significant deposition on the surface of quartz plates. Deposition of NP on the electordes surface was registered at a level of 5 % of the total mass of the removed target material.

The obtained magnetic NP together with the gold NP were used at the final stage, the purpose of which was to form composite magneto-plasmon NP with the „core-satellites“ configuration as a result of ultrasonic exposure to a solution obtained by mixing two types of NP (Fig. 1, *c*). In the „core“ — magnetic NP, „satellite“ configuration — golden NP on the surface of „core“. The source of ultrasonic exposure in this experiment was an immersion dispersant UZTA-0,1/28-O (Center for Ultrasound Technologies, Biysk), with its maximum intensity of ultrasound exposure 300 W/cm^2 with ultrasonic vibration frequency (28 ± 2.5) kHz, tip diameter 4.5 mm. Ultrasonic exposure intensity was 240 W/cm^2 (80 % of the maximum), in order to avoid overheating during ultrasonic exposure, the tube with the solution was placed in a vessel filled with cold water and ice, the duration of ultrasonic exposure was 20 min. At the end of the process, a magnetic separation step was performed to separate the composite magneto-plasmon NP from the gold NP that did not react with the magnetic NP.

In the experiments on synthesis of composite iron and gold NP, where a colloidal solution of gold NP and a solution of magnetic NP obtained by laser ablation of iron in argon (zero valent iron (ZVI) (Fe^0)) in the alpha-iron phase (α-Fe)) were used as components, an additional step was needed to functionalize the NP α-Fe. When magentic particles obtained by laser ablation of iron in the air served as magnetic component the functionalization stage was skipped. Thus, the solution of α-Fe NP was prepared by transferring NP synthesized by laser ablation method of iron in argon stored in acetone, into ethanol (95 %). Then polyvinylpyrrolidone K30 (PVP, M.W. 40,000) was added to the NP test tube, the PVP concentration in the solution was 10 mg/ml, this procedure was necessary to modify the surface of NP in order to reduce the likelihood of NP oxidation when interacting with an oxygen-containing medium and increase the colloidal stability of NP. The test tube with the resulting solution was placed in an ultrasonic bath for 60 min, then the unbound PVP was cleaned by magnetic separation of NP and rinsing with ethanol (twice), and then with deionized water (once). At the final stage, deionized water was replaced with a colloidal solution of gold NP, so the prepared solution contained PVP modified nanoparticles α-Fe and gold NP. Then, the solution was subjected to ultrasonic exposure using an immersion dispersant, and after that a magnetic separation was performed. It was found that after sampling the magnetic NP, the solution had a saturated red color, which evidenced that some of the gold NP did not react with the magnetic NP, which raises the question of choosing the optimal ratio of NP in the solution prior to the ultrasound exposure.

2. Results and discussion

The morphology of synthesized nanoparticles was studied using a scanning electron microscope (SEM) (Quanta 200 3D, FEI), the sizes of NP were defined manually by analyzing the SEM images. Fig. 2, *a*, *c* shows SEM images of magnetic NP obtained by laser ablation of iron in air and composite iron and gold NP, which were obtained as a result of three-stage synthesis, respectively. The appropriate hystograms of the particles size distribution are shown in Fig. 2, *b*, *d*.

This method provides the formation of composite NP having the „core-satellites“ configuration (unevenly distributed gold NP directly on the surface of larger magnetic NP). It should be stressed that the NP average size decreased as a result of ultrasonic exposure, e.g., the NP prepared at the second stage (laser ablation of iron in air) had an average size of 104 nm, and at the end of the third stage, the average size decreased by half and amounted to 50 nm. The electrostatic attraction of differently charged particles is probably one of the possible mechanisms for the formation of composite nanoparticles of the „core–satellites“ configuration. If NP surface has different charge the golden NP are coated with iron NP. When exposed to ultrasound, the contact of differently charged NP becomes more likely, thus ensuring an effective process of forming the composite

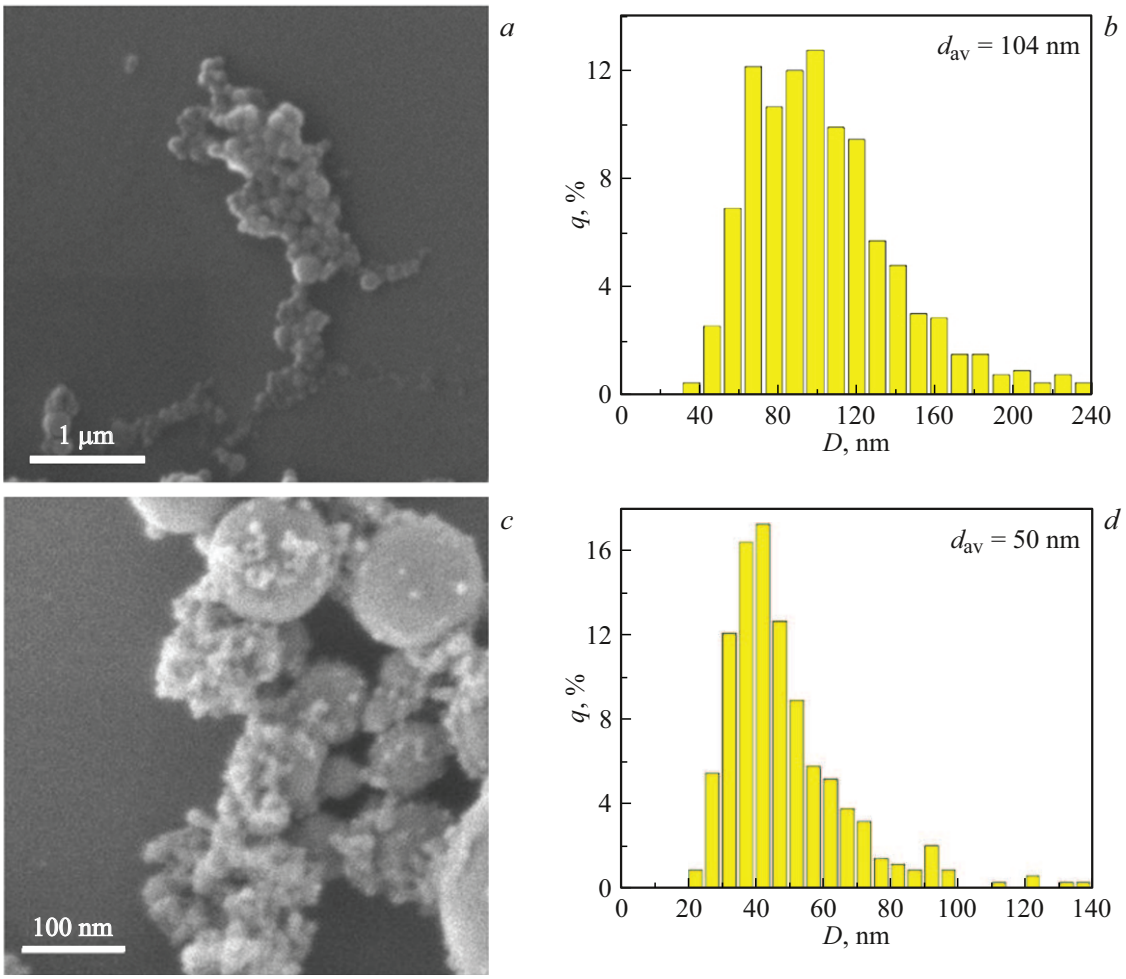

Figure 2. SEM images and histograms of particle size distribution: magnetic NP obtained by laser ablation of iron in air (a, b); composite NP based on iron and gold obtained by three-stage synthesis (c, d).

NP. In addition, acoustic cavitation (formation, growth and destruction of gaseous microbubbles) and special conditions that occur during ultrasonic processing can contribute to the formation of composite NP due to various mechanical effects [21]. The decrease in the NP size as a result of ultrasonic exposure is probably due to mechanical action, which leads to deagglomeration of particles and their fragmentation, while the presence of defects in the surface of NP makes the fragmentation process more likely.

The X-ray diffractometry method was used to study the structural features and chemical composition of synthesized NP. The particles were analyzed by a powder X-ray diffractometer Bruker D9 ADVANCE (Bruker, Germany), the radiation source was the long-focal tube CuKα (wavelength of $\lambda = 1.542$ Å). Figure 3 shows diffraction patterns of composite iron and gold NP obtained as a result of three-stage synthesis by laser ablation and auxiliary ultrasound exposure: magnetic NP were obtained by laser ablation of iron in air (Fig. 3,it a); magnetic NP were obtained by laser ablation of iron in argon (Fig. 3, b).

Fig. 3, a illustrates the presence of diffraction peaks at 30.46, 35.76, 37.38, 43.4, 53.78, 57.25, 62.82, 74.3, 87.32, 89.96 deg, which correspond to the scattering on the lattice planes with an orientation (220), (311), (222), (400), (422), (511), (440), (533), (622), (642) and (731) magnetite (Fe_3O_4) and/or maghemite (γ-Fe_2O_3) respectively [22]. This set of peaks and their intensity almost completely coincide with the diffraction pattern observed for magnetic NP synthesized by laser ablation in air (the presence of the Fe_3O_4 phase was confirmed by Raman scattering, no other phases were detected). In addition, there are peaks at 38.49, 44.71, 64.91 and 78.02 deg, related to the planes (111), (200), (220) and (311) gold (Au) [23], which were also observed in the case of composite NP obtained by a two-stage ablative synthesis in a liquid medium [18]. The peak at 69.3 deg relates to the silicon plane (400) (silicon wafer where the nanopratciles were deposited). In Fig. 3, b, diffraction peaks can be observed at 44.81, 65.24, 82.48 deg, which correspond to the planes (110), (200) and (211) α-Fe [24], this set of peaks coincides with a diffraction pattern of magnetic NP synthesized by laser ablation in

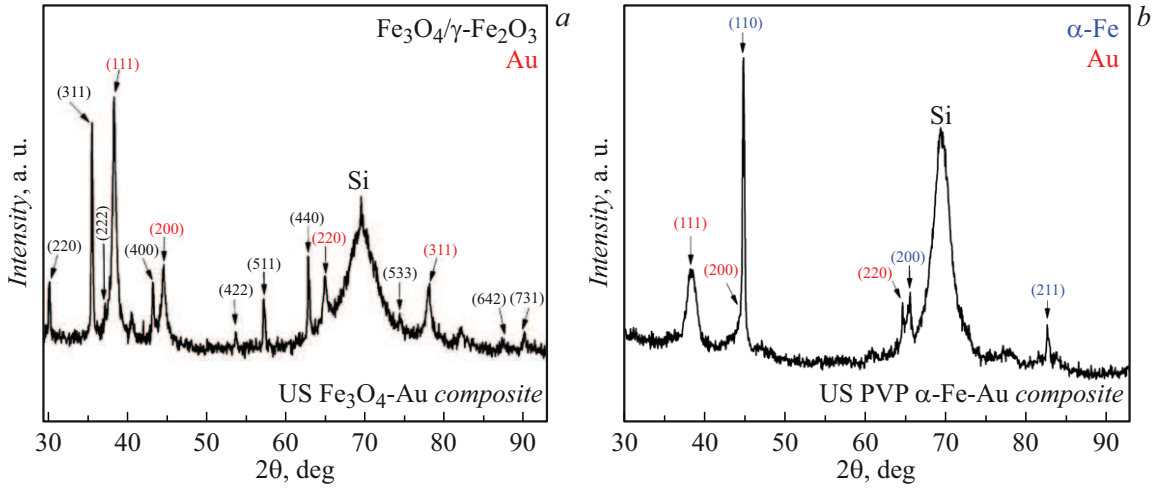

Figure 3. Diffraction patterns of composite iron and gold NP obtained as a result of three-stage synthesis by laser ablation and auxiliary ultrasound exposure: magnetic NP were obtained by laser ablation of iron in air (*a*); magnetic NP were obtained by laser ablation of iron in argon (*b*).

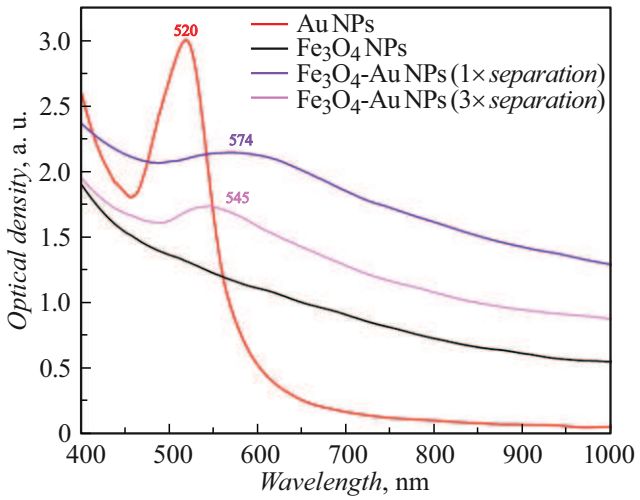

Figure 4. Optical density curves of gold NP solution (red curve); Fe_3O_4 NP solution (black curve) synthesized by laser ablation in air (liquid medium —deionized water); solutions of composite Fe_3O_4–Au nanoparticles obtained by ultrasonic exposure after one (purple curve) and three stages of magnetic separation (pink curve).

argon, which proves that the initial phase of magnetic NP after ultrasonic exposure is preserved. Also, the peaks at 38.48, 44.68, 64.75 deg, associated with planes (111), (200), (220) of gold are present.

The optical properties of the obtained colloidal solutions were studied by spectrophotometry using SF-2000 spectrophotometer (OKB-Spektr, Russia). The measurements were carried out in quartz cuvettes with an optical path length of 10 mm. Fig. 4 illustrates the optical density curves of the gold NP solution, Fe_3O_4 NP solution synthesized by laser ablation in air (liquid medium —deionized water); solutions of composite NP Fe_3O_4–Au obtained as a result of ultrasonic exposure after one and three stages of magnetic separation.

A redshift of the plasmon resonance position from 520 to 574 nm is observed for a solution after one stage of magnetic separation. While for a solution, after three stages of magnetic separation, the position of the plasmon resonance shifts to 545 nm while maintaining an extended arm extending into the long-wavelength region of the spectrum.

Prior to the measurements of optical properties the solutions were 5 times diluted. The optical density curves of gold NP solutions, PVP NP of α-Fe, composite PVP NP of α-Fe–Au and non-reacted gold NP (pink curve), are illustrated in Fig. 5, *a*. Figure 5, *b* shows a photo of colloidal solutions of gold NP and composite NP. Fig. 5, *c* shows a photo of colloidal solutions of gold NP and composite NP 1 min after the introduction of a permanent magnet.

The plasmon resonance for composite NP shifts towards 548 nm, and in general, the observed spectral pattern bears a strong resemblance to the earlier described specifics of composite NP.

3. Photohermal properties of composite NP based on iron and gold

Experiments related to measurement of the photothermal response of the obtained colloidal systems were carried out according to the scheme shown in Fig. 6.

As a radiation source *1* a semiconductor laser diode was used, generating continuous infrared radiation at a wavelength of 805 nm. A collimator was used to convert a diverging beam into a collimated one *2*. The collimated beam *3* passed through the side wall of a quartz cuvette *4* (wall thickness 1 mm, optical path length 10 mm) filled

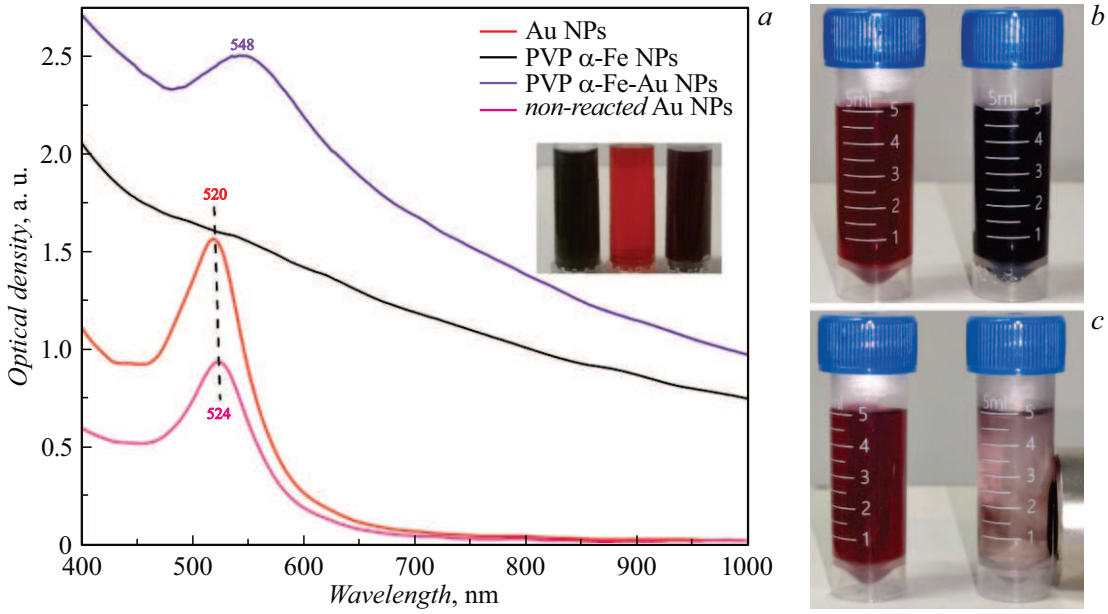

Figure 5. Optical density curves of solutions of gold NP (red curve), PVP NP of α-Fe (black curve), composite PVP NP of α-Fe–Au (purple curve) and non-reacted gold NP (pink curve), photo in the insert - colloidal solutions (from left to right: PVP NP α-Fe; gold NP; composite NP PVP α-Fe–Au) (*a*); photo of colloidal solutions of gold NP (in the left) and composite NP (in the right) (*b*); photo of colloidal solutions of gold NP (in the left) and composite NP 1 min after introduction of permanent magnet (in the right) (*c*).

with 1 ml of colloidal solution. Next, the power of radiation passed through the solution cuvette was measured, a thermoelectric sensor *5* and a power meter were used for this; here, the thermoelectric sensor was placed behind the cuvette at a distance of about 5 mm from its nearest face. The kinetics of heating the colloidal solution as a result of irradiation was measured using a thermal imaging camera *6*, temperature readings were taken from the side surface of the cuvette in the area of radiation transmission, and the process was recorded on camera. The analysis of video recordings of thermal imaging was carried out using ImageJ software, changes in the temperature of the colloidal solution were recorded every 10 seconds. The temperature of the solutions prior to irradiation in all experiments was 23 °C, the temperature variation (ΔT) was calculated as the difference between the current temperature and the initial value. In experiments to measure the photothermal response, the irradiation power was 0.7W.

The optical density curves of NP solutions and the corresponding graphs of temperature variation versus time under continuous laser irradiation for these solutions are shown in Fig. 7. The same colors of the curves on the fragment (Fig. 7, *a*) and the graphs of temperature dependence on the fragments (Fig. 7, *b*, *c*) were used specifically for unambiguous comparison of optical and photothermal properties of solutions. Fig. 7, *b* shows the curves of temperature variation versus time during irradiation of composite NP colloidal solutions formed by the method of a two-stage laser synthesis as described in [18], and three-stage synthesis, where the magnetic component was the NP obtained by laser ablation of iron in air, concentration of

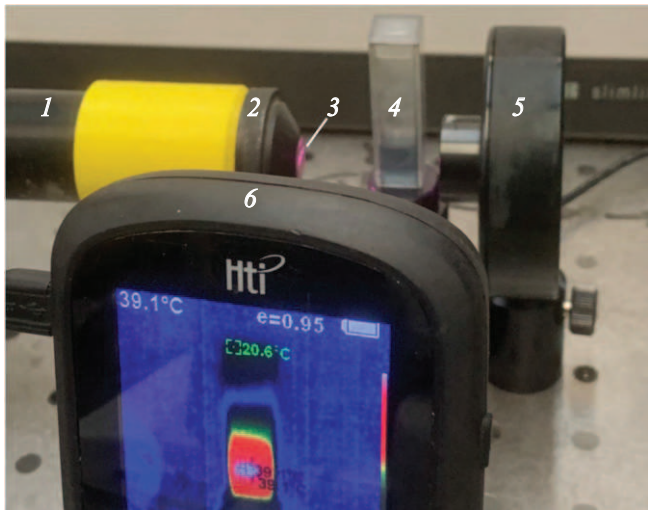

Figure 6. A stand for measuring the photothermal properties of colloidal solutions.

solutions was ~ 0.6 mg/ml. Curves of temperature variation versus time during irradiation of PVP NP colloidal solutions α-Fe and composite PVP NP solutions of α-Fe–Au of various concentrations are given in Fig. 7, *c*.

As can be seen in Fig. 7, *b*, the dynamics of heating solutions obtained by various methods practically coincide. The tempeature growth makes 10.8 °C and 10.6 °C for the 2-stage laser synthesis and 3-stage synthesis, accordingly. The highest temperature growth was observed for the PVP NP solution of α-Fe (concentration ~ 0.1 mg/ml) and

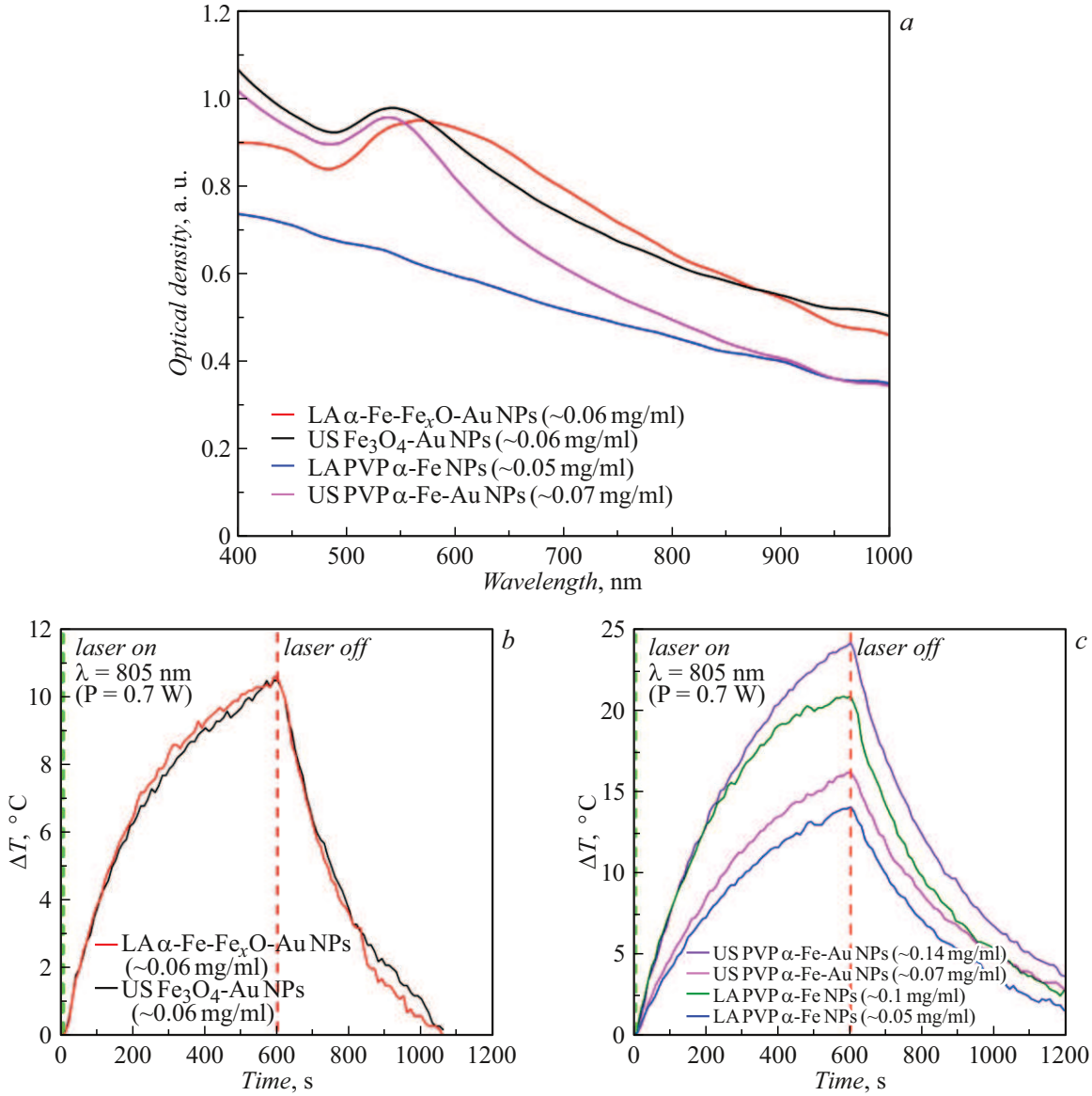

Figure 7. Optical density curves of NP solutions of Fe–Fe$_x$O–Au (red curve), Fe$_3$O$_4$–Au (black curve), PVP α-Fe (blue curve) and PVP α-Fe–Au (pink curve) (*a*). Curves of temperature variation versus time for the irradiated colloidal solutions: composite NP of Fe–Fe$_x$O–Au and Fe$_3$O$_4$–Au (red and black curves) (*b*); NP PVP of α-Fe (blue and green curves) and composite NP PVP of α-Fe–Au (pink and violet curves) (*c*).

composite PVP NP solution of α-Fe–Au (concentration ~ 0.14 mg/ml), heating was up to 20.9 °C and 24.2 °C accordingly. At lower concentration 0.05 mg/ml for the PVP NP solution of α-Fe and 0.07 mg/ml for the composite PVP NP solution of α-Fe–Au, the temperature increased by 14.1 °C and 16.2 °C, respectively, after irradiation.

Conclusion

The study demonstrates a successful realization of an integrated approach to the synthesis of composite magneto-plasmon nanoparticles with controlled structure and properties. The obtained materials have a high photothermal potential and can be used as multifunctional agents in biomedical and optical applications. The experimental data obtained (SEM, X-ray diffraction and spectrophotometry data) prove the potential use of the proposed combined approach to create composite nanoparticles with magnetic and plasmonic properties. This approach allows to flexibly vary the synthesis conditions to obtain the NP with the necessary properties.

As a result, a universal combined method of synthesis of composite NP with a „core–satellite“ configuration with controlled properties has been developed. The average size of the nanoparticles decreased from 104 to 50 nm after ultrasonic treatment, which indicates deagglomeration and fragmentation of particles. The use of polyvinylpyrrolidone

made it possible to stabilize the NP α-Fe and prevent their oxidation. X-ray phase analysis of composite magneto-plasmon NP of two different types confirmed the presence of magnetite/maghemite and gold phases, as well as α-Fe and gold, respectively. For the two types of considered composite NP, a redshift of the plasmon resonance position from 520 to 545−548 nm is observed, indicating an interaction between gold and magnetic NP.

When irradiating the composite magneto-plasmon NP colloidal solutions Fe_3O_4-Au and PVP NP solutions α-Fe–Au with concentrations of 0.06 and 0.07 mg/ml by continuous laser with a wavelength of 805 nm the heating was 10.6 °C and 16.2 °C respectively. The observed photothermal response rises with increasing concentration of solutions, which indicates the possibility of regulating the degree of local heating, an important condition for potential use in photothermal therapy.

Funding

The study of the processes of formation of nanoparticles and assembly of experimental setups were supported by the grant from the Russian Science Foundation (grant № 24-12-20015). The preparation and analysis of samples was carried out within the state assignment of the Ministry of Science and Higher Education of Russian Federation (thesis FZUN-2024-0019.)

Conflict of interest

The authors declare that they have no conflict of interest.

References

[1] A.A. Popov, Z. Swiatkowska-Warkocka, M. Marszalek, G. Tselikov, I.V. Zelepukin, A. Al-Kattan, S.M. Deyev, S.M. Klimentov, T.E. Itina, A.V. Kabashin. Nanomaterials, **12** (4), 649 (2022). DOI: 10.3390/nano12040649
[2] P. Hu, S. Zhang, T. Wu, D. Ni, W. Fan, Y. Zhu, R. Qian, J. Shi. Adv. Mater., **30** (31), 1801690 (2018). DOI: 10.1002/adma.201801690
[3] A. Basagni, V. Torresan, P. Marzola, M.B.F. van Raap, L. Nodari, V. Amendola. Faraday Discuss., **242**, 286 (2023). DOI: 10.1039/D2FD00087C
[4] Q. Gu, J. Zhu, G.J. Weng, J.J. Li, J.W. Zhao. Microchim. Acta, **189** (12), 470 (2022). DOI: 10.1007/s00604-022-05559-0
[5] D.C. Luther, R. Huang, T. Jeon, X. Zhang, Y.W. Lee, H. Nagaraj, V.M. Rotello. Adv. Drug Deliv. Rev., **156**, 188 (2020). DOI: 10.1016/j.addr.2020.06.020
[6] A.S. Gonçalves, C.F. Rodrigues, A.F. Moreira, I.J. Correia. Acta Biomater., **116**, 105 (2020). DOI: 10.1016/j.actbio.2020.09.008
[7] S. Hossen, M.K. Hossain, M.K. Basher, M.N.H. Mia, M.T. Rahman, M.J. Uddin. J. Adv. Res., **15**, 1 (2019). DOI: 10.1016/j.jare.2018.06.005
[8] A. Mittal, I. Roy, S. Gandhi. Magnetochem., **8** (9), 107 (2022). DOI: 10.3390/magnetochemistry8090107
[9] H. Gavilán, S.K. Avugadda, T. Fernández-Cabada, N. Soni, M. Cassani, B.T. Mai, R. Chantrell, T. Pellegrino. Chem. Soc. Rev., **50** (20), 11614 (2021). DOI: 10.1039/D1CS00427A
[10] O.Y. Griaznova, I.B. Belyaev, A.S. Sogomonyan, I.V. Zelepukin, G.V. Tikhonowski, A.A. Popov, A.S. Komlev, P.I. Nikitin, D.A. Gorin, A.V. Kabashin, S.M. Deyev. Pharmaceutics, **14** (5), 994 (2022). DOI: 10.3390/pharmaceutics14050994
[11] J. Kadkhoda, A. Tarighatnia, J. Barar, A. Aghanejad, S. Davaran. Photodiagnosis Photodyn. Ther., **37**, 102697 (2022). DOI: 10.1016/j.pdpdt.2021.102697
[12] A.B. Bucharskaya, N.G. Khlebtsov, B.N. Khlebtsov, G.N. Maslyakova, N.A. Navolokin, V.D. Genin, E.A. Genina, V.V. Tuchin. Materials, **15** (4), 1606 (2022). DOI: 10.3390/ma15041606
[13] A. Sood, V. Arora, J. Shah, R.K. Kotnala, T.K. Jain. Mater. Sci. Eng. C, **80**, 274 (2017). DOI: 10.1016/j.msec.2017.05.079
[14] M. Muniz-Miranda, F. Muniz-Miranda, E. Giorgetti. Nanomaterials, **10** (1), 132 (2020). DOI: 10.3390/nano10010132
[15] N.G. Semaltianos, G. Karczewski. ACS Appl. Nano Mater., **4** (7), 6407 (2021). DOI: 10.1021/acsanm.1c00715
[16] A.A. Laktionov, I.V. Sozaev, D.I. Tselikov, G.V. Tikhonovskii, M.S. Grigor'yeva, S.M. Klimentov, I.N. Zavestovskaya, A.V. Kabashin, A.A. Popov. Bull. Lebedev Phys. Inst., **51** (Suppl 7), S602 (2024). DOI: 10.3103/S1068335624601821
[17] M. Jelić, E. Mühlhausen, M. Kamp, F. Pohl, S. Riegg, M. Wickleder, G. Beck. Nano Struct. Nano-Objects, 39, 101246 (2024). DOI: 10.1016/j.nanoso.2024.101246
[18] U.E. Kurilova, A.S. Chernikov, D.A. Kochuev, L.S. Volkova, A.A. Voznesenskaya, R.V. Chkalov, D.V. Abramov, A.V. Kazak, I.A. Suetina, M.V. Mezentseva, L.I. Russu, A.Yu. Gerasimenko, K.S. Khor'kov. Biomed. Eng., **58**, 106 (2024). DOI: 10.1007/s10527-024-10376-1
[19] A.S. Chernikov, D.A. Kochuev, M.A. Dzus, A.A. Voznesenskaya, U.E. Kurilova, R.V. Chkalov, A.V. Kazak, A.Yu. Gerasimenko, K.S. Khorkov. FTT, **66** (12), 2210 (2024) (in Russian). DOI: 10.61011/FTT.2024.12.59597.6290PA
[20] U.E. Kurilova, A.S. Chernikov, D.A. Kochuev, L.S. Volkova, A.A. Voznesenskaya, R.V. Chkalov, D.V. Abramov, A.V. Kazak, I.A. Suetina, M.V. Mezentseva, L.I. Russu, A.Yu. Gerasimenko, K.S. Khorkov. J. Biomed. Photonics Eng., **9** (2), 020301 (2023). DOI: 10.18287/JBPE23.09.020301
[21] C. Devos, A. Bampouli, E. Brozzi, G.D. Stefanidis, M. Dusselier, T. Van Gerven, S. Kuhn, Chem. Society Rev., **54** (1), 85 (2025). DOI: 10.1039/D4CS00148F
[22] E.A. Moacă, C.G. Watz, V. Socoliuc, R. Racoviceanu, C. Păcurariu, R. Ianoş, S. Cîntă-Pînzaru, L.B. Tudoran, F. Nekvapil, S. Iurciuc, C. Şoica, C.A. Dehelean. Nanomaterials, **11** (5), 1189 (2021). DOI: 10.3390/nano11051189
[23] M. Sedki, G. Zhao, S. Ma, D. Jassby, A. Mulchandani, Sensors, **21** (3), 883 (2021). DOI: 10.3390/s21030883
[24] Y. Hirano, Y. Kasai, K. Sagata, Y. Kita. Bull. Chem. Society Jpn., **89** (9), 1026 (2016). DOI: 10.1246/bcsj.20160114

Translated by T.Zorina